



CHORUS

This is the accepted manuscript made available via CHORUS. The article has been published as:

Quantum spin transfer torque induced nonclassical magnetization dynamics and electron-magnetization entanglement

Priyanka Mondal, Utkarsh Bajpai, Marko D. Petrović, Petr Plecháč, and Branislav K. Nikolić

Phys. Rev. B **99**, 094431 — Published 21 March 2019

DOI: [10.1103/PhysRevB.99.094431](https://doi.org/10.1103/PhysRevB.99.094431)

Quantum spin-transfer torque induced nonclassical magnetization dynamics and electron-magnetization entanglement

Priyanka Mondal,¹ Utkarsh Bajpai,¹ Marko D. Petrović,² Petr Plecháč,² and Branislav K. Nikolić^{1, *}

¹*Department of Physics and Astronomy, University of Delaware, Newark, DE 19716, USA*

²*Department of Mathematical Sciences, University of Delaware, Newark, DE 19716, USA*

The standard spin-transfer torque (STT)—where spin-polarized current drives dynamics of magnetization viewed as a classical vector—requires noncollinearity between electron spins carried by the current and magnetization of a ferromagnetic layer. However, recent experiments [A. Zholud *et al.*, Phys. Rev. Lett. **119**, 257201 (2017)] observing magnetization dynamics in spin valves at cryogenic temperatures, even when electron spin is collinear to magnetization, point at overlooked quantum effects in STT which can lead to *highly nonclassical* magnetization states. Using quantum many-body treatment, where an electron injected as spin-polarized wave packet interacts with local spins comprising the anisotropic quantum Heisenberg ferromagnetic chain, we define *quantum STT as any time evolution of local spins due to initial many-body quantum state not being an eigenstate of electron+local-spins composite system*. For time evolution caused by injected spin- \downarrow electron scattering off local \uparrow -spins, *entanglement* between electron and local spins subsystems takes place leading to *decoherence* and, therefore, shrinking of the total magnetization but without rotation from its initial orientation, which explains the experiments. Furthermore, the same processes—entanglement and thereby induced true decoherence—are present even in the standard noncollinear geometry, intertwined with the usual magnetization rotation. This is because STT in quantum many-body picture is always caused by electron spin- \downarrow factor state, and the only difference between collinear and noncollinear geometries is in relative size of the contribution of the initial separable state containing such factor to superposition of separable many-body quantum states generated by time evolution.

The standard spin-transfer torque (STT)¹, predicted in the seminal works of Slonczewski² and Berger³, is a phenomenon where a flux of spin-polarized electrons injected into a ferromagnetic metal (FM) layer drives its magnetization dynamics. The origin of STT is transfer of spin angular momentum from electrons to local magnetic moments of the FM layer, so it is fundamentally a nonequilibrium quantum many-body physics effect. Nevertheless, local magnetic moments $\mu_S \mathbf{S}(\mathbf{r})$ are typically treated as *classical vectors of fixed length*^{1,4} whose dynamics is governed by the Landau-Lifshitz-Gilbert (LLG) equation⁵ extended by adding the STT term⁶⁻⁸

$$\mathbf{T} \propto \langle \hat{\mathbf{s}}_e \rangle \times \mathbf{S}(\mathbf{r}). \quad (1)$$

Thus, the nonequilibrium spin density $\langle \hat{\mathbf{s}}_e \rangle$ caused by the flowing electrons *must be noncollinear* to the direction of local spin $\mathbf{S}(\mathbf{r})$, to drive magnetization dynamics in such a classical picture. The dynamics can include oscillations or complete reversal, whose conversion into resistance variations has emerged as a key resource for next generation spintronic technologies, such as nonvolatile magnetic random access memories, microwave oscillators, microwave detectors, spin-wave emitters, memristors and artificial neural networks⁹⁻¹¹.

For example, passing current through a spin valve trilayer fixed-FM/normal-metal/free-FM, as employed in early experiments on standard STT^{12,13}, causes first FM layer with fixed magnetization to spin-polarize the current which then impinges onto the second FM layer with free magnetization that fluctuates in the classical picture due to a random magnetic field caused by thermal motion. When impinging spins and fluctuating magnetization become noncollinear, standard STT can either

amplify such fluctuations (for fixed-to-free spin current direction) or reduce them (for free-to-fixed spin current direction), as predicted theoretically¹⁴ and confirmed experimentally¹⁵ at room temperature.

However, this well-established picture *cannot* explain very recent experiments¹⁶ on collinear spin valves at cryogenic temperatures $\lesssim 3$ K, where resistance measurements have revealed magnetization dynamics even though thermal fluctuations that could introduce noncollinearity between the free and fixed magnetizations are suppressed. This implies a mechanism where standard STT is zero, $\mathbf{T} \equiv 0$ in Eq. (1), so that magnetization does not rotate from the the initial configuration. Nevertheless, it changes its length, thereby signaling generation of *highly nonclassical* magnetization states¹⁶. However, the proposed intuitive picture¹⁶ where such mechanism would amplify quantum spin fluctuations, for both fixed-to-free and free-to-fixed spin current directions, cannot be rigorously justified. That is, although quantum fluctuations of the local spin operators¹⁷ (or, equivalently, zero-point energy of magnons as bosonic particles to which spin operators can be mapped) play an important role in lowering the energy of classical ground states of antiferromagnets¹⁸ or noncollinear spin textures¹⁹, they *vanish* in a FM with uniaxial anisotropy because the collinear state of local magnetic moments is also a ground eigenstate of the exact Hamiltonian²⁰.

Aside from few disparate attempts²¹⁻²³, a general framework for describing current-driven *quantum dynamics* of magnetization is lacking. Note that quantum transport theories, such as the nonequilibrium Green function formalism^{7,8,24,25} or the scattering matrix approach^{26,27}, are routinely used to compute $\langle \hat{\mathbf{s}}_e \rangle$ in Eq. (1) for a given

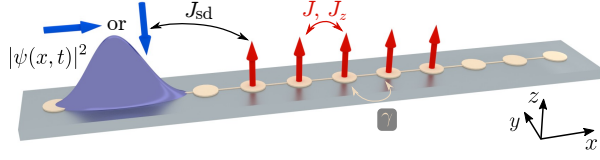


FIG. 1. Schematic view of a quantum many-body system consisting of a FM layer whose $N = 5$ local spins comprise the open XXZ quantum Heisenberg ferromagnetic chain with anisotropic exchange interactions $J_z > J$, and are attached to 1D TB chain (composed of $L_x = 400$ sites) where electron hops with parameter γ . The spin-polarized electron wave packet is injected along the TB chain, with its spin pointing in the $-z$ - or $+x$ -direction which is collinear [a case where the standard STT of Slonczewski² and Berger³ in Eq. (1) is absent] or noncollinear, respectively, to local spins pointing initially along the $+z$ -direction. The spin of the wave packet interacts with local spins via s - d exchange interaction J_{sd} .

single-particle Hamiltonian, but this serves only as an input^{7,8} for the LLG equation describing classical dynamics of magnetization. The LLG equation can be justified under the assumptions⁵ of large spin $S \rightarrow \infty$, $\hbar \rightarrow 0$ (while $S \times \hbar \rightarrow 1$) and in the *absence of entanglement*. The latter assumption means that local spins comprising the total magnetization should remain in a separable quantum state, $|S_1\rangle \otimes |S_2\rangle \otimes \dots \otimes |S_N\rangle$, as exemplified by the ground state of a FM, $|\uparrow\rangle \otimes |\uparrow\rangle \otimes \dots \otimes |\uparrow\rangle$.

Instead of classical micromagnetics^{4,14} or quantum-classical^{7,8} description of standard-STT-induced magnetization dynamics, here we introduce a quantum many-body picture of *both* flowing-electron-spin-local-spins interactions and the ensuing time evolution of local spins at zero temperature. For this purpose, we employ a system depicted in Fig. 1 where spin-polarized electron wave packet, assumed to originate from a fixed FM layer, is injected along one-dimensional (1D) tight-binding (TB) chain whose sites in the middle host local spins comprising a quantum Heisenberg ferromagnetic chain modeling the free FM layer. The states of such composite quantum system electron+local-spins reside in the Hilbert space

$$\mathcal{H} = \mathcal{H}_{\text{orb}}^e \otimes \mathcal{H}_{\text{spin}}^e \otimes \mathcal{H}_{\text{spin}}^1 \otimes \dots \otimes \mathcal{H}_{\text{spin}}^N, \quad (2)$$

which is the tensor product of orbital electron subspace $\mathcal{H}_{\text{orb}}^e$ (of finite dimension equal to the number of sites L_x of the TB chain); two-dimensional subspace $\mathcal{H}_{\text{spin}}^e$ for electron spin; and $\mathcal{H}_{\text{spin}}^n$ as two-dimensional subspaces for $n = 1, \dots, N$ local spins assumed to be spin- $\frac{1}{2}$ as well. The system Hamiltonian acting in \mathcal{H} is

$$\begin{aligned} \hat{H} = & -\gamma \sum_{\langle ij \rangle} |i\rangle \langle j| - J_{sd} \sum_i |i\rangle \langle i| \otimes \hat{\mathbf{s}}_e \cdot \hat{\mathbf{S}}_i(t) \\ & - \sum_{\langle ij \rangle} \left[J(\hat{S}_i^x \cdot \hat{S}_j^x + \hat{S}_i^y \cdot \hat{S}_j^y) + J_z \hat{S}_i^z \cdot \hat{S}_j^z \right], \quad (3) \end{aligned}$$

where $|i\rangle$ is electron orbital centered on site i ; $\gamma = 1$ eV is hopping between nearest-neighbor sites; and

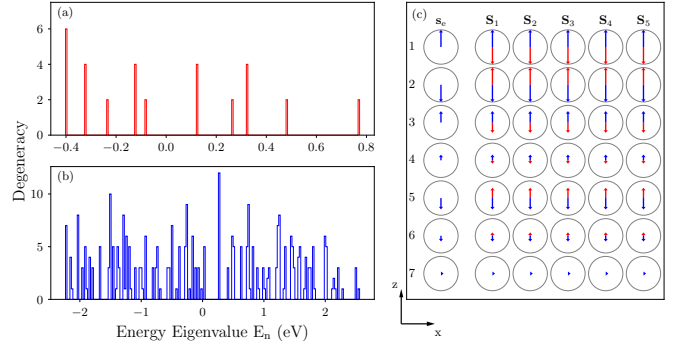


FIG. 2. (a) Eigenspectrum of the XXZ quantum Heisenberg ferromagnetic chain whose $N = 5$ local spins in Fig. 1 do not interact with electron spin ($J_{sd} = 0$). (b) Eigenspectrum of many-body Hamiltonian in Eq. (3) whose local spins interact via s - d interaction ($J_{sd} = 0.1$ eV) with electron spin within TB chain of length $L_x = 400$. (c) Expectation value of electron spin (first column) and local spins, extracted from their subsystem density matrices via Eq. (6), in the degenerate ground state of the lowest energy in panel (a) [red arrows] or (b) [blue arrows].

$J_{sd} = 0.1$ eV is the strength of s - d exchange interaction between electron and local spins. The exchange interaction between the nearest neighbor local spins is $J = 0.1$ eV and $J_z = 0.1005$ eV, which are slightly different in order to include the uniaxial anisotropy, quantified by the parameter $\Delta = J_z/J$ ^{28,29}, with the z -axis as the easy axis. The third term in Eq. (3) is denoted as the XXZ quantum Heisenberg ferromagnetic chain with *open* boundary conditions (due to first and last spin interacting with only one nearest-neighbor spin)^{28,29}. The spin operators in Eq. (3) are constructed as $\hat{\mathbf{s}}_e = \hat{I} \otimes \hat{\boldsymbol{\sigma}} \otimes \hat{I} \otimes \dots \otimes \hat{I}$ for electron spin; $\hat{\mathbf{S}}_1 = \hat{I} \otimes \hat{I} \otimes \hat{\boldsymbol{\sigma}} \otimes \hat{I} \otimes \dots \otimes \hat{I}$ for first local spins and analogously for all other local spins, where $\hat{\boldsymbol{\sigma}} = (\hat{\sigma}_x, \hat{\sigma}_y, \hat{\sigma}_z)$ is the vector of the Pauli matrices and \hat{I} is the unit operator. The eigenspectrum of an isolated XXZ chain is shown in Fig. 2(a), while the eigenspectrum of the whole many-body Hamiltonian in Eq. (3) is shown in Fig. 2(b). The ground state in the former (latter) case has degeneracy six (seven), as shown in Fig. 2(c) and expected for a system of coupled five (six) spin- $\frac{1}{2}$ angular momenta.

At $t = 0$, the many-body quantum state is a separable one

$$\langle x | \Psi(t=0) \rangle = C e^{ik_x x - \delta k_x^2 x^2 / 4} \otimes \chi_e \otimes \chi_1 \otimes \dots \otimes \chi_N. \quad (4)$$

Its first factor in $\mathcal{H}_{\text{orb}}^e$ is chosen as a Gaussian wave packet with momentum along the $+x$ -direction and centered on the left edge of TB chain, as illustrated in Fig. 1, where C is the normalization constant. To mimic current of electrons at the Fermi level which interact with the ground state of free FM layer within a spin valve, we use $k_x a = 0.1$ and $\delta k_x a = 0.2$ (a is the lattice spacing) which tune wave packet average energy $E = -2.36$ eV and its standard deviation $\delta E = 0.054$ eV to be close to

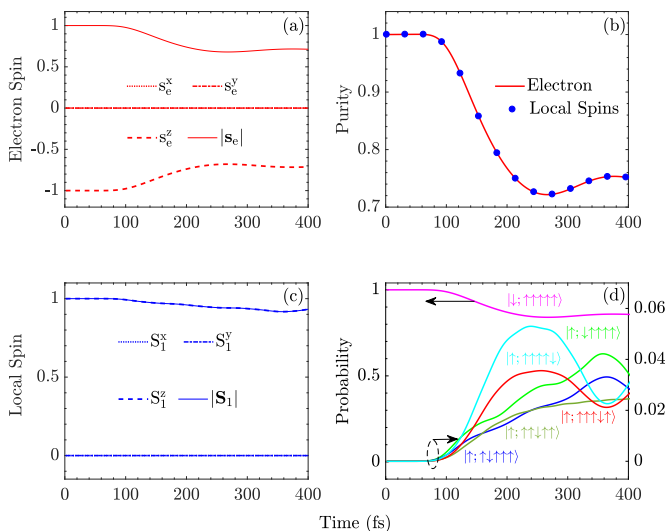


FIG. 3. Time dependence of the expectation value of spin (in units $\hbar/2$) obtained from spin- $\frac{1}{2}$ density matrix in Eq. (6) for: (a) spin of injected electron wave packet in Fig. 1 which at $t = 0$ points in the $-z$ -direction that is *collinear* and antiparallel to local spins pointing in the $+z$ -direction; and (c) first local spin in Fig. 1 [time dependence of expectation value of local spins $n = 2-5$ is nearly identical to (c)]. (b) Purity defined in Eq. (7) of the subsystem composed of electron degrees of freedom (orbital and spin) or of the subsystem composed of all local spins. (d) Probability in Eq. (8) to find electron-spin+local-spins subsystem in many-body quantum state $|\sigma_e; \sigma_1\sigma_2\sigma_3\sigma_4\sigma_5\rangle$.

the ground state eigenenergy $E_0 = -2.43$ eV [Fig. 2(b)] of the Hamiltonian in Eq. (3). In the ground state, all local spins are aligned with the anisotropy z -axis, as shown in Fig. 2(c), so we choose $\chi_n = \begin{pmatrix} 1 \\ 0 \end{pmatrix}$ for $n = 1, \dots, N$. To mimic *minority* spin electrons impinging onto the free FM layer within a spin valve with parallel magnetizations, we select initial spin polarization of the wave packet in the $-z$ -direction, as described by the spinor $\chi_e = \begin{pmatrix} 0 \\ 1 \end{pmatrix}$. For the standard STT setup with noncollinear magnetizations of the fixed and free FM layers, we use spin polarization in the $+x$ -direction, $\chi_e = \frac{1}{\sqrt{2}} \begin{pmatrix} 1 \\ 1 \end{pmatrix}$.

For transparency of the discussion, operating with a small number of excited states of the XXZ chain which can be analyzed one by one, we employ small number $N = 5$ of local spins. The chosen length $L_x = 400$ of the TB chain ensures that wave packet does not reflect from its boundaries within the time frame considered in Figs. 3 and 4. The *numerically exact* $|\Psi(t)\rangle$, governed by the Schrödinger equation $i\hbar\partial|\Psi(t)\rangle/\partial t = \hat{H}|\Psi(t)\rangle$, is obtained by using the Crank-Nicolson algorithm³⁰.

Figure 2(c) shows that degenerate ground state has electron and local spins parallel to each other due to s - d interaction between them acting to align them.

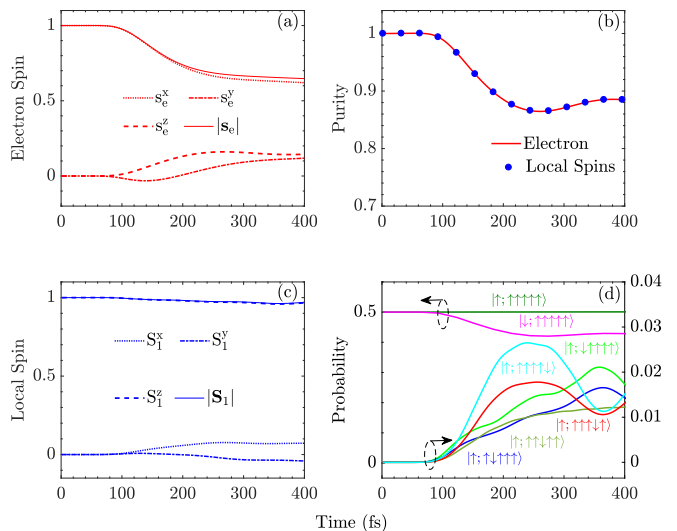


FIG. 4. Panels (a)–(d) plot the same information as panels (a)–(d), respectively, in Fig. 3 but for injected electron wave packet which at $t = 0$ is spin-polarized in the $+x$ -direction, i.e., *noncollinear* to local spins pointing in the $+z$ -direction.

Thus, when an electron with spin- \downarrow along the $-z$ -direction is injected, its spin is collinear to local spins but $|\Psi(t=0)\rangle \equiv |G\rangle \otimes |\downarrow_e; \uparrow_1 \dots \uparrow_N\rangle$ (this form is used below for economy of notation) at $t = 0$ is not an eigenstate of the Hamiltonian in Eq. (3). *This causes time evolution of the electron-spin+local-spins subsystem, which rigorously defines quantum STT even in situation where the standard STT in Eq. (1) is identically zero.* In the course of time evolution, $|\Psi(t)\rangle$ becomes an entangled state due to linear superpositions of separable states being generated for $t > 0$. The entanglement entails that each subsystem must be described using the appropriate reduced density matrix³¹

$$\hat{\rho}_{\text{sub}} = \text{Tr}_{\text{other}} |\Psi(t)\rangle\langle\Psi(t)|, \quad (5)$$

obtained via partial trace applied to the pure state density matrix $|\Psi(t)\rangle\langle\Psi(t)|$. For example, tracing over the states in the subspace $\mathcal{H}_{\text{orb}}^e \otimes \mathcal{H}_{\text{spin}}^e \otimes \mathcal{H}_{\text{spin}}^2 \dots \otimes \mathcal{H}_{\text{spin}}^N$ yields the density matrix of first local spin

$$\hat{\rho}_1(t) = \frac{1}{2} [\hat{I} + \mathbf{S}_1(t) \cdot \hat{\boldsymbol{\sigma}}], \quad (6)$$

where $\mathbf{S}_1(t) = \text{Tr}[\hat{\rho}_1(t)\hat{\boldsymbol{\sigma}}]$ is the spin expectation value (in units of $\hbar/2$), also denoted as the polarization (or Bloch) vector³¹. Pure (or fully coherent) quantum states of spin- $\frac{1}{2}$ are characterized by $|\mathbf{S}_1| = 1$, while $0 < |\mathbf{S}_1| < 1$ signifies their decoherence^{31,32} toward mixed (or partially coherent³⁴) states. Figure 3(c) shows that first local spin has $S_1^z < 1$, $S_1^x = S_1^y \equiv 0$ and, therefore, $|\mathbf{S}_1| < 1$. The electron spin also exhibits decoherence, $|s_e| < 1$, in Fig. 3(a). Virtually the same time-dependences as in Fig. 3(c) are obtained for other local spins $i = 2, \dots, 5$, and, therefore, for total magnetization as the sum of local spins. Thus, this is precisely the highly nonclassical state

of magnetization conjectured from the measurement of the spin valve resistance¹⁶, which increases $\propto 1 - M_z$ due to magnetization $M_z = g\mu_B \sum_i S_i^z$ shrinking without rotation (i.e., $M_x = M_y = 0$) away from its initial orientation.

To explain the origin of magnetization decoherence, or, equivalently, of the subsystem comprised of *all* local spins, we view multipartite [due to $N + 2$ factors in Eq. (2)] total system as a bipartite one, i.e., as being composed of the electron subsystem whose states reside in $\mathcal{H}_{\text{orb}}^e \otimes \mathcal{H}_{\text{spin}}^e$ and the subsystem of all local spins. The purity of the latter is defined as^{31,32}

$$\mathcal{P}_{\text{spins}}^{\text{local}}(t) = \text{Tr} \{ [\hat{\rho}_{\text{spins}}^{\text{local}}(t)]^2 \}, \quad (7)$$

where density matrix $\hat{\rho}_{\text{spins}}^{\text{local}}(t)$ is obtained via Eq. (5) by tracing over the states in the subspace $\mathcal{H}_{\text{orb}}^e \otimes \mathcal{H}_{\text{spin}}^e$. The decay of $\mathcal{P}_{\text{spins}}^{\text{local}}(t)$ below one in Fig. 3(b) quantifies *true decoherence*^{32,33} (i.e., the decoherence which cannot be attributed to any classical fluctuations) of initially pure state $|\uparrow\rangle \otimes |\uparrow\rangle \otimes \dots \otimes |\uparrow\rangle$ as the decay^{31,32} of the off-diagonal elements of $\hat{\rho}_{\text{spins}}^{\text{local}}(t)$ caused by entanglement with the electron subsystem. The purity of decohered electron subsystem in Fig. 3(b) is identical to that of the local spin subsystem, as expected for entanglement in bipartite quantum systems^{31,32}.

To understand the states of electron-spin+local-spins subsystem which are excited during time evolution initiated by injection of a single spin-polarized electron, we compute the density matrix $\hat{\rho}_{\text{spins}}^{\text{e+local}}(t)$ of this subsystem obtained by partial trace in Eq. (5) performed over the states in $\mathcal{H}_{\text{orb}}^e$. The probability to find this subsystem in state $|\sigma_e; \sigma_1 \dots \sigma_N\rangle$ at time t

$$\text{prob}_{\text{spins}}^{\text{e+local}}(t) = \langle \sigma_e; \sigma_1 \dots \sigma_N | \hat{\rho}_{\text{spins}}^{\text{e+local}}(t) | \sigma_e; \sigma_1 \dots \sigma_N \rangle, \quad (8)$$

is shown in Fig. 3(d) for electron injected with spin along the $-z$ -direction. The subspace of \mathcal{H} whose states can generate nonzero $\text{prob}_{\text{spins}}^{\text{e+local}}(t)$ is restricted by the energy bands in Fig. 2(b) [caused by anisotropy and boundaries^{28,29}] and symmetries, such as that total spin in the z -direction has to be conserved due to its operator, $\hat{S}_{\text{tot}}^z = \hat{s}^z + \hat{S}_1^z + \dots + \hat{S}_N^z$, commuting with the Hamiltonian in Eq. (3), $[\hat{H}, \hat{S}_{\text{tot}}^z] = 0$. Because of the latter requirement, all states $|\sigma_e; \sigma_1 \dots \sigma_N\rangle$ participating in time evolution must have the same number of \uparrow -spins, so that one finds in Fig. 3(d) progressive excitation of states with flipped spin of an electron and one flipped local spin with a total transfer of angular momentum of $1 \times \hbar$. However, the initial state $|\downarrow; \uparrow \dots \uparrow\rangle$ maintains its probability close to one, and other states with flipped electron spin and one flipped local spin have much smaller and nonuniform probability (note that increased probability to find $|\uparrow; \uparrow\uparrow\uparrow\downarrow\rangle$ state is a consequence of XXZ chain being open which brings this state and $|\uparrow; \downarrow\uparrow\uparrow\uparrow\rangle$ state into resonance^{28,29}). Such peculiar quantum superposition of separable many-body states, with large contribution from the initial state, leads to local spins

maintaining their direction along the z -axis in Fig. 3(c). This can be contrasted with naïve (i.e., not taking into account superpositions) intuition^{22,35} where spin- \downarrow electron simply flips first local spin—the flip then propagates to displace transversally other local spins away from the anisotropy axis, eventually exciting white spectrum²² of lowest-energy magnons^{28,29}.

The same effects—entanglement of electron state and quantum state of all local spins [Fig. 4(b)]; thereby induced true decoherence^{32,33} of electron spin [Fig. 4(a)] and local spins [Fig. 4(c)]; and high probability [Fig. 4(d)] to find initial state of electron-spin+local-spins subsystem in the course of time evolution—are present also in the standard STT geometry with noncollinearity between spin of the injected electron and local spins. However, in the standard STT geometry we also find the usual magnetization rotation, i.e., $S_1^x \neq 0$ and $S_1^y \neq 0$ in Fig. 4(c). The probabilities $\text{prob}_{\text{spins}}^{\text{e+local}}(t)$ in Fig. 4(d) to excite states of the type $|\uparrow; \uparrow \dots \downarrow \dots \uparrow\rangle$ are simply half of those obtained for collinear geometry in Fig. 3(d) since spin of the injected electron along the $+x$ -direction used in Fig. 4 means $|\rightarrow_e\rangle = \frac{1}{\sqrt{2}}(|\uparrow_e\rangle + |\downarrow_e\rangle)$ where only $\frac{1}{\sqrt{2}}|\downarrow_e\rangle$ term, entering as a factor of the initial separable many-body state $|\Psi(t=0)\rangle \equiv |G\rangle \otimes \frac{1}{\sqrt{2}}(|\uparrow_e\rangle + |\downarrow_e\rangle) \otimes |\uparrow_1 \dots \uparrow_N\rangle$, induces time evolution of local spins and transfer of angular momentum. On the other hand, $\frac{1}{\sqrt{2}}|\uparrow_e\rangle \otimes |\uparrow_1 \dots \uparrow_N\rangle$ term in the initial many-body state is an eigenstate [Fig. 2(c)] of electron-spin+local-spins subsystem and, therefore, has time-independent $\text{prob}_{\text{spins}}^{\text{e+local}}(t) = 1/2$ in Fig. 4(d). Thus, identical profile of curves in Figs. 3(d) and 4(d) reveal that *in fully quantum many-body picture there is no difference between the standard STT and quantum STT*—both originate from $|\downarrow_e\rangle$ factor state brought into the initial many-body state by either minority spin electrons³⁵ in spin valves with parallel magnetizations¹⁶, or by $|\downarrow_e\rangle$ term in the quantum superposition of electron spin states generated by polarizing effect of the fixed magnetization that is noncollinear to free magnetization.

We note that increasing the total number of local spins from $N = 5$ considered here to realistic large values does not change these findings due to Schmidt decomposition³⁶ which makes it possible to re-write *any* entangled state of spin- $\frac{1}{2}$ as the sum of just two terms, $a|\nearrow\rangle \otimes |\Sigma_1\rangle + b|\searrow\rangle \otimes |\Sigma_2\rangle$, where $|\Sigma_{1,2}\rangle \in \mathcal{H}_{\text{spin}}^1 \dots \otimes \mathcal{H}_{\text{spin}}^N$. Thus, the Schmidt decomposition state looks the same as the entangled state of spin- $\frac{1}{2}$ with just a single macrospin. We provide counterparts of Figs. 3 and 4 in the Appendix where a single local spin- $\frac{5}{2}$ is employed as the macrospin.

We emphasize that piecewise-linear increase of differential resistance with the bias voltage observed in Ref.¹⁶ and our explanation of its origin cannot be accounted by inelastic electron-magnon scattering³⁷ often observed in magnetic tunnel junctions which actually leads to opposite effect where differential resistance of the junction with collinear magnetizations (parallel or antiparallel) decreases^{38,39} with the bias voltage due to opening of

additional conduction channels³⁷.

Our model in Fig. 1 can be viewed as an addition to the atlas of toy models considered in Ref.²⁶ to explain conventional STT of Slonczewski² and Berger³ due to a *single* injected spin-polarized electron in plane wave orbital state which is treated quantum-mechanically, while the magnetization receiving the torque is treated as a classical vector of fixed length. In contrast, in our toy model of Fig. 1 *both* the single injected spin-polarized electron, in wave packet orbital state, and localized spins receiving the torque are treated as a single quantum many-body system. However, to explain conventional STT in realistic junctions requires to also sum over incoming momenta of all Fermi surface electrons^{26,27}, which reduces the transverse component of the transmitted and reflected spin currents to nearly zero due to substantial phase cancellation^{26,27}, so that conventional STT is very nearly proportional to the transverse piece of the incident spin current. While such effect is not considered in our strictly one-dimensional system (in three-dimensional spin valves, one sums different incident transverse wave vectors that are parallel to junction interfaces^{26,27}), we do effectively include averaging over different momenta of plane waves comprising the wave packet. We relegate to future studies investigation of nonclassical state of magnetization interacting with a flux of electrons with different momenta arising from different parts of the Fermi surface.

Finally, during the completion of this work we became aware of two studies^{40,41} where magnetization dynamics in collinear spin valves at cryogenic temperatures is treated quantum-mechanically to find quantum STT on a single macrospin signified by $\langle S_z \rangle \neq 0$ while $\langle S_x \rangle = \langle S_y \rangle = 0$. However, these studies do not invoke entanglement-induced true decoherence mechanism we discuss (for the case of macrospin in Appendix A). Instead, Ref.⁴⁰ invokes equilibrium quantum spin fluctuations⁴⁰ [which is incorrect, i.e., $1/2$ contribution in Eq. (1) of Ref.⁴⁰, due to “vacuum fluctuations” or zero-point energy, is *forbidden* in the ground state of ferromagnets¹⁸⁻²⁰] combined with random magnetic field⁴² by the nonequilibrium spin shot noise⁴⁰. On the other hand, Ref.⁴¹ invokes inelastic electron-magnon scattering to find differential resistance of a magnetic tunnel junction with parallel collinear magnetizations which increases with the bias voltage at low temperatures, in contrast to prior experiments^{38,39} where such resistance decreases with the bias voltage at low temperatures.

ACKNOWLEDGMENTS

We are grateful to D. Ralph, M. Stiles and S. Urazhdin for instructive discussions. P. M., U. B. and B. K. N. were supported by NSF Grant No. ECCS 150909. M. P. and P. P. were supported by ARO MURI Award No. W911NF-14-0247.

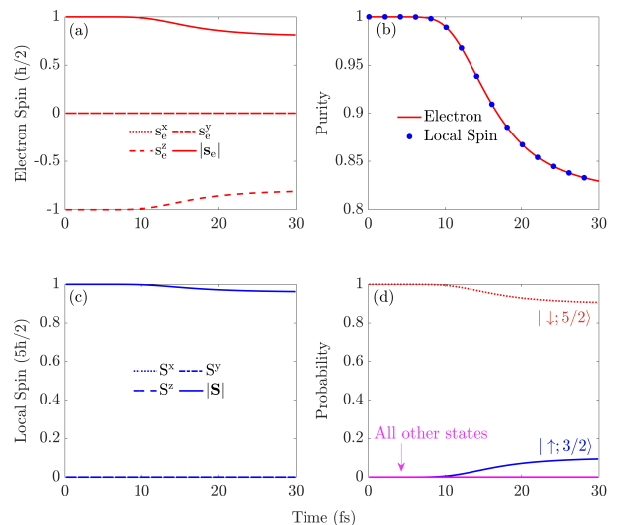


FIG. 5. Time dependence of the expectation value of spin (in units $\hbar/2$) obtained from respective density matrices for: (a) spin of injected electron wave packet which at $t = 0$ points in the $-z$ -direction that is *collinear* and antiparallel to a single local spin- $\frac{5}{2}$ pointing in the $+z$ -direction; and (c) local spin- $\frac{5}{2}$. (b) Purity defined in Eq. (7) for the subsystem composed of electron degrees of freedom (orbital and spin) or of the subsystem composed of all local spins. (d) Probability in Eq. (8) to find electron-spin+local-spin subsystem in many-body quantum state $|\sigma_e; S_z\rangle$

Appendix A: Quantum description of spin-transfer torque and the ensuing dynamics of single macrospin

In this Appendix, we provide additional Figs. 5 and 6, as the counterparts of Figs. 3 and 4, respectively, for injected spin-polarized electron wave packet whose spin interacts via s - d exchange interaction with a macrospin representing the active ferromagnetic layer that receives spin-transfer torque (STT). Note that this Appendix can also be viewed as a rigorous analysis of heuristic arguments provided in Section III.B of the Supplemental Material of Ref.¹⁶.

The macrospin is modeled using a single (i.e., $N = 1$ in Fig. 1) local spin- $\frac{5}{2}$. Since we assume absence of spin-orbit coupling, the orbital state of the wave packet, $|G\rangle$, and the state of electron-spin+local-spins subsystem, $|\text{spins}\rangle$, remain uncorrelated³¹ in the course of time evolution, $|\Psi(t)\rangle = |G\rangle \otimes |\text{spins}\rangle$.

In the case of $|G\rangle \otimes |\uparrow\rangle$ injected electron wave packet, with electron spin pointing in the $+z$ -direction, and local spin- $\frac{5}{2}$ being collinear to it in the state $|S_z = 5/2\rangle$, there is no any STT or entanglement since $|\Psi(t)\rangle = |G\rangle \otimes |\uparrow\rangle \otimes |5/2\rangle$ is a separable eigenstate of the many-body Hamiltonian and, therefore, does not change with time.

In the case of $|G\rangle \otimes |\downarrow\rangle$ injected electron wave packet, with electron spin pointing in the $-z$ -direction and local spin- $\frac{5}{2}$ being collinear in state $|S_z = 5/2\rangle$, initial and final

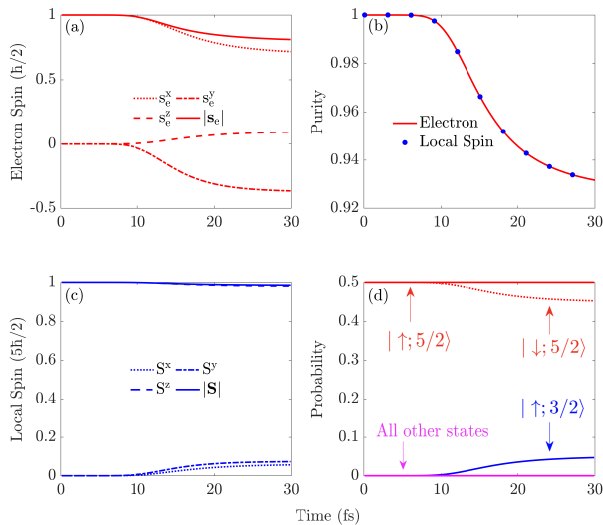


FIG. 6. Panels (a)–(d) plot the same information as panels (a)–(d), respectively, in Fig. 5 but for injected electron wave packet which at $t = 0$ is spin-polarized in the $+x$ -direction, i.e., *noncollinear* to local spin- $\frac{5}{2}$ pointing in the $+z$ -direction.

states are given by

$$|\Psi(t = 0)\rangle = |G\rangle \otimes |\downarrow\rangle \otimes |5/2\rangle, \quad (\text{A.1a})$$

$$|\Psi(t > 0)\rangle = a(t)|G\rangle \otimes |\downarrow\rangle \otimes |5/2\rangle + b(t)|G\rangle \otimes |\uparrow\rangle \otimes |3/2\rangle, \quad (\text{A.1b})$$

where time-evolution of probabilities in Fig. 5(d) is given

by $|a(t)|^2$ (red dotted line) and $|b(t)|^2$ (blue solid line). The total spin in the z -direction remains conserved during time evolution. In the course of time evolution, local spin- $\frac{5}{2}$ in Fig. 5(c) *does not* rotate away from the z -axis, but it is shrinking due to true decoherence caused by entanglement in Eq. (A.1b).

In the case of $|G\rangle \otimes \frac{1}{\sqrt{2}}(|\uparrow\rangle + |\downarrow\rangle)$ injected electron wave packet, with electron spin pointing in the $+x$ -direction and local spin- $\frac{5}{2}$ pointing in the $+z$ -direction in the state $|S_z = 5/2\rangle$, initial and final states are given by

$$|\Psi(t = 0)\rangle = |G\rangle \otimes \frac{1}{\sqrt{2}}(|\uparrow\rangle + |\downarrow\rangle) \otimes |5/2\rangle, \quad (\text{A.2a})$$

$$|\Psi(t > 0)\rangle = \frac{1}{\sqrt{2}}|G\rangle \otimes |\uparrow\rangle \otimes |5/2\rangle + \frac{a(t)}{\sqrt{2}}|G\rangle \otimes |\downarrow\rangle \otimes |5/2\rangle + \frac{b(t)}{\sqrt{2}}|G\rangle \otimes |\uparrow\rangle \otimes |3/2\rangle, \quad (\text{A.2b})$$

where time evolution of probabilities in Fig. 6(d) is given by $1/2$ (red solid line), $|a(t)|^2/2$ (red dotted line) and $|b(t)|^2/2$ (blue solid line). The latter two are just half of the probabilities in Fig. 5(d). In the course of time evolution, this change leads to local spin- $\frac{5}{2}$ in Fig. 6(c) *both* rotating away from the z -axis, as in the standard STT of Slonczewski² and Berger³, and shrinking due to true decoherence caused by entanglement in Eq. (A.2b). The former effect is the same as the only consequence of quantum STT in Fig. 5(c).

* bnkolic@udel.edu

¹ D. Ralph and M. Stiles, Spin transfer torques, *J. Magn. Magn. Mater.* **320**, 1190 (2008).
² J. C. Slonczewski, Current-driven excitation of magnetic multilayers, *J. Magn. Magn. Mater.* **159**, L1 (1996).
³ L. Berger, Emission of spin waves by a magnetic multilayer traversed by a current, *Phys. Rev. B* **54**, 9353 (1996).
⁴ D. V. Berkov and J. Miltat, Spin-torque driven magnetization dynamics: Micromagnetic modeling, *J. Magn. Magn. Mater.* **320**, 1238 (2008).
⁵ R. Wieser, Description of a dissipative quantum spin dynamics with a Landau-Lifshitz-Gilbert like damping and complete derivation of the classical Landau-Lifshitz equation, *Euro. Phys. J. B* **88**, 77 (2015).
⁶ A. Manchon, N. Ryzhanova, A. Vedyayev, M. Chshiev, and B. Dieny, Description of current-driven torques in magnetic tunnel junctions, *J. Phys.: Condens. Matter* **20**, 145208 (2008).
⁷ M. D. Petrović, B. S. Popescu, U. Bajpai, P. Plecháč, and B. K. Nikolić, Spin and charge pumping by a steady or pulse-current-driven magnetic domain wall: A self-consistent multiscale time-dependent quantum-classical hybrid approach, *Phys. Rev. Applied* **10**, 054038 (2018).
⁸ M. O. A. Ellis, M. Stamenova, and S. Sanvito, Multiscale modeling of current-induced switching in magnetic tunnel junctions using *ab initio* spin-transfer torques, *Phys. Rev.*

B **96**, 224410 (2017).

⁹ N. Locatelli, V. Cros, and J. Grollier, Spin-torque building blocks, *Nat. Mater.* **13**, 11 (2014).
¹⁰ A. D. Kent and D. C. Worledge, A new spin on magnetic memories, *Nat. Nanotech.* **10**, 187 (2015).
¹¹ W. A. Borders, H. Akima, S. Fukami, S. Moriya, S. Kurihara, Y. Horio, S. Sato, and H. Ohno, Analogue spin-orbit torque device for artificial-neural-network-based associative memory operation, *Appl. Phys. Expr.* **10**, 013007 (2017).
¹² M. Tsoi, A. G. M. Jansen, J. Bass, W. C. Chiang, V. Tsoi, and P. Wyder, Generation and detection of phase-coherent current-driven magnons in magnetic multilayers, *Nature* **406**, 46 (2000).
¹³ J. A. Katine, F. J. Albert, R. A. Buhrman, E. B. Myers, and D. C. Ralph, Current-driven magnetization reversal and spin-wave excitations in Co/Cu/Co pillars, *Phys. Rev. Lett.* **84**, 3149 (2000).
¹⁴ Z. Li and S. Zhang, Thermally assisted magnetization reversal in the presence of a spin-transfer torque, *Phys. Rev. B* **69**, 134416 (2004).
¹⁵ R. H. Koch, J. A. Katine, and J. Z. Sun, Time-resolved reversal of spin-transfer switching in a nanomagnet, *Phys. Rev. Lett.* **92**, 088302 (2004).
¹⁶ A. Zholud, R. Freeman, R. Cao, A. Srivastava, and S. Urazhdin, Spin transfer due to quantum magnetization

- fluctuations, Phys. Rev. Lett. **119**, 257201 (2017).
- ¹⁷ Y. Takahashi, *Spin Fluctuation Theory of Itinerant Electron Magnetism* (Springer, Berlin, 2013).
 - ¹⁸ A. Singh and Z. Tešanović, Quantum spin fluctuations in an itinerant antiferromagnet, Phys. Rev. B **41**, 11457 (1990).
 - ¹⁹ A. Roldán-Molina, M. J. Santander, A. S. Núñez, and J. Fernández-Rossier, Quantum fluctuations stabilize skyrmion textures, Phys. Rev. B **92**, 245436 (2015).
 - ²⁰ K. Yosida, *Theory of Magnetism* (Springer, Berlin, 1996).
 - ²¹ Y. Wang and L. J. Sham, Quantum dynamics of a nanomagnet driven by spin-polarized current, Phys. Rev. B **85**, 092403 (2012); Y. Wang, and L. J. Sham, Quantum approach of mesoscopic magnet dynamics with spin transfer torque, Phys. Rev. B **87**, 174433 (2013); T. Tay and L. J. Sham, Theory of atomistic simulation of spin-transfer torque in nanomagnets, Phys. Rev. B **87**, 174407 (2013).
 - ²² J. P. Gauyacq and N. Lorente, Excitation of spin waves by tunneling electrons in ferromagnetic and antiferromagnetic spin- $\frac{1}{2}$ Heisenberg chains, Phys. Rev. B **83**, 035418 (2011); J. P. Gauyacq and N. Lorente, Magnetic reversal of a quantum nanoferrromagnet, Phys. Rev. B **87**, 195402 (2013).
 - ²³ F. Mahfouzi and N. Kioussis, Current-induced damping of nanosized quantum moments in the presence of spin-orbit interaction, Phys. Rev. B **95**, 184417 (2017).
 - ²⁴ P. M. Haney, D. Waldron, R. A. Duine, A. S. Núñez, H. Guo, and A. H. MacDonald, Current-induced order parameter dynamics: Microscopic theory applied to Co/Cu/Co spin valves, Phys. Rev. B, **76**, 024404 (2007).
 - ²⁵ B. K. Nikolić, K. Dolui, M. Petrovi, P. Plecháč, T. Markussen, and K. Stokbro, First-principles quantum transport modeling of spin-transfer and spin-orbit torques in magnetic multilayers, in W. Andreoni and S. Yip (eds.), *Handbook of Materials Modeling* (Springer, Cham, 2019); [arXiv:1801.05793](https://arxiv.org/abs/1801.05793).
 - ²⁶ M. D. Stiles and A. Zangwill, Anatomy of spin-transfer torque, Phys. Rev. B **66**, 014407 (2002).
 - ²⁷ S. Wang, Y. Xu, and K. Xia, First-principles study of spin-transfer torques in layered systems with noncollinear magnetization, Phys. Rev. B **77**, 184430 (2008).
 - ²⁸ M. Haque, Self-similar spectral structures and edge-locking hierarchy in open-boundary spin chains, Phys. Rev. A **82**, 012108 (2010).
 - ²⁹ K. Joel, D. Kollmar, and L. F. Santos, An introduction to the spectrum, symmetries, and dynamics of spin-1/2 Heisenberg chains, Am. J. Phys. **81**, 450 (2013).
 - ³⁰ J. E. Bayfield, *Quantum Evolution: An Introduction to Time-Dependent Quantum Mechanics* (Wiley, New York, 1999).
 - ³¹ L. E. Ballentine, *Quantum Mechanics: A Modern Development* (World Scientific, Singapore, 2014).
 - ³² E. Joos, H. D. Zeh, C. Kiefer, D. J. W. Giulini, J. Kupsch, and I. Stamatescu, *Decoherence and the Appearance of a Classical World in Quantum Theory* (Springer, Berlin, 2003).
 - ³³ J. Kayser, K. Luoma, and W. T. Strunz, Geometric characterization of true quantum decoherence, Phys. Rev. A **92**, 052117 (2015).
 - ³⁴ B. K. Nikolić and S. Souma, Decoherence of transported spin in multichannel spin-orbit-coupled spintronic devices: Scattering approach to spin-density matrix from the ballistic to the localized regime, Phys. Rev. B **71**, 195328 (2005).
 - ³⁵ T. Balashov, A. F. Takács, M. Däne, A. Ernst, P. Bruno, and W. Wulfhekel, Inelastic electron-magnon interaction and spin transfer torque, Phys. Rev. B **78**, 174404 (2008).
 - ³⁶ A. Ekert and P. L. Knight, Entangled quantum systems and the Schmidt decomposition, Am. J. Phys. **63**, 415 (1995).
 - ³⁷ F. Mahfouzi and B. K. Nikolić, Signatures of electron-magnon interaction in charge and spin currents through magnetic tunnel junctions: A nonequilibrium many-body perturbation theory approach, Phys. Rev. B **90**, 045115 (2014).
 - ³⁸ J. C. Slonczewski and J. Z. Sun, Theory of voltage-driven current and torque in magnetic tunnel junctions, J. Magn. Mater. **310**, 169 (2007).
 - ³⁹ V. Drewello, J. Schmalhorst, A. Thomas, and G. Reiss, Evidence for strong magnon contribution to the TMR temperature dependence in MgO based tunnel junctions, Phys. Rev. B **77**, 014440 (2008).
 - ⁴⁰ A. Qaiumzadeh and A. Brataas, Quantum magnetization fluctuations via spin shot noise, Phys. Rev. B **98**, 220408(R) (2018).
 - ⁴¹ S. A. Bender, R. A. Duine, and Y. Tserkovnyak, Quantum spin-transfer torque and magnon-assisted transport in nanostructures, Phys. Rev. B **99**, 024434 (2019).
 - ⁴² A. L. Chudnovskiy, J. Swiebodzinski, and A. Kamenev, Spin-torque shot noise in magnetic tunnel junctions, Phys. Rev. Lett. **101**, 066601 (2008).